Optical Crosstalk Improvement in Ring Resonator Based Add/Drop Multiplexers Using Controllable Reflectivity

Riyadh D. Mansoor [1] and Alistair P. Duffy [2]

[1] Engineering College
Al-Muthanna University, Samawa, Iraq
riyadhdmu@mu.edu.iq

[2] School of Engineering and Sustainable Development
De Montfort University, Leicester, UK
apd@dmu.ac.uk

Abstract ─ In this paper, the topic of optical signal integrity is approached by studying crosstalk suppression in ring resonator based optical Add/Drop Multiplexers (OADM). The resonance splitting induced by surface corrugation is exploited to enhance signal integrity by increasing the crosstalk suppression bandwidth compared to that of a smooth-walled resonator. Sidewall roughness in silicon-on-insulator waveguides is studied using Coupled Mode Theory (time and space domain CMT). An analytical model of a corrugated ring resonator is presented, which is then exploited to estimate the spectral response of the different ports. Verification against results generated from full-wave electromagnetic numerical modeling of a randomized corrugated ring is performed. The analysis then examines the performance of an OADM with controllable reflectivity resulting from a predefined corrugation of sidewall. Gratings have been successfully used in optical filters; this paper proposes the use of a grating in an OADM, giving more controlled roughness. A grating-assisted design of a single ring OADM with 28 GHz crosstalk suppression bandwidth is presented. This bandwidth supports the dropping of 10 Gbps signals with mitigated crosstalk levels and improved signal integrity.

Index Terms ─ Back reflection, crosstalk, grating reflectivity, ring resonators, sidewall roughness.

I. INTRODUCTION

Signal integrity issues in all optical networks are of increasing interest due to the closer proximity of waveguides and optical components as integration density increases. The distinction between RF and optical communications frequencies is diminishing, making true on the claim that Electromagnetic compatibility (EMC) is "a DC to light phenomenon". Silicon-On-Insulator (SOI) is a promising technology to increase the integration density of all optical networks [1], [2]. SOI waveguides provide high confinement of light in devices of small dimensions and allow for large-scale integration in planar light wave circuits [3]. In this technology the propagation loss is relatively low [4]. However, the back-reflection effect due to sidewall roughness is of great importance [5], [6]. In rough-walled ring resonators, back reflection is a well-known cause of resonance splitting due to the interference between forward and counter-directional modes [7]-[9]. This effect has been exploited to increase the extinction ratio by enhancing the depth of the through port response at resonance [7]. In this paper, the resonance splitting resulting from a periodic perturbation of the sidewall roughness is exploited to improve the crosstalk performance of optical add/drop multiplexers OADMs in wavelength division multiplexed (WDM) networks by increasing the crosstalk suppression bandwidth [10].

Back reflection is a frequency dependent phenomenon that manifests as a variation of the response at each resonant frequency. The existence of resonance splitting relies on the relation between coupling coefficients and reflectivity. To extract the coupling and loss coefficients from experimental or numerical results, the back-reflection effect should be considered to produce an accurate analysis of OADMs. A coherent backscattering measuring system [11] and a fully analytical model [4] have been proposed to characterize all parameters of the ring including back reflection.

The sidewall roughness was created using semi-periodic gratings as reported, experimentally, in [12]. A set of ridges having identical length and period was shown to act as a wall corrugation. Therefore, it was studied as a quasi-grating and the reflectivity was measured as a function of frequency. Controlling the backscattering by predefining the dimensions of a quasi-grating during the fabrication introduces a new field of applications using grating-assisted resonators [13], [14]. Using Bragg grating calculations [15], the back-reflection

Submitted On: January 18, 2019
Accepted On: May 6, 2019

effect can be controlled by changing the grating dimensions (number, period and lengths of gratings). The dual-mode filter model has been used recently in photonic integrated platforms [16] in a similar manner to that in microwave circuits. Using a partial reflector inside a single ring resonator will result in a second order response. This effect has been exploited to enhance filter performance [9] and maximize the bandwidth of crosstalk suppression [17].

In this paper, controllable levels of back-reflection induced by a periodic surface corrugation are exploited to improve the crosstalk suppression bandwidth. This bandwidth of crosstalk suppression is defined as the bandwidth over which the suppression of intra-band crosstalk is maintained above 20 dB [18]. To achieve this aim, the research presented in this paper is arranged as follows:

1. Time domain Coupled Mode Theory (CMT) [19], [20] is exploited to propose an analytical model. This model allows a complete characterization of all parameters of the ring including back reflection.

2. An equivalent model of the corrugated ring is presented. The back-reflection can be visualized as resulting from a virtual ring. The space domain calculation is used, where the sidewall roughness is treated as a single scattering point.

3. The validity of the proposed models is tested against an existing experimental result [4]. Time and space domain models allow for accurate characterization of the ring without the need for curve fitting calculations.

4. The spectral response of different ports is simulated numerically using a commercial full wave simulation tool, CST [21], and the controllable reflectivity induced by semi-periodic gratings is modelled and validated using the ASPIC design simulator [22].

This paper presents a general solution for rough-wall ring resonator modelling as well as a particular solution to maximize the crosstalk suppression bandwidth. It concludes with a design that provides a 28 GHz crosstalk bandwidth.

II. COUPLED MODE ANALYSIS

Mutual coupling between the back reflected mode (induced by surface corrugation) and the forward mode is modelled analytically using CMT (coupled mode theory), both in the time and space domains.

A. Time domain analysis

Starting with Fig. 1, $a(t)$ is the forward mode, while $b(t)$ refers to the back-reflection mode, which is related to $a(t)$ through the reflection coefficient *r*. No new channels at the add port were assumed.

Based on the analysis of the time domain CMT [7], [23], the stored energy in the ring (forward mode) behaves as described by eq. (1):

$$\frac{\mathrm{da(t)}}{\mathrm{dt}} = \left(\mathrm{j}\omega_0 - \frac{1}{\tau}\right)\cdot \mathrm{a(t)} - \mathrm{j}k_1 \cdot \mathrm{S_i} - \mathrm{ju}\cdot \mathrm{b(t)}. \quad (1)$$

Where $u = \sqrt{\mathrm{r}}\cdot\frac{\mathrm{V_g}}{\mathrm{l}}$, is the mutual coupling, l is the perimeter of resonator $(2\pi R)$, V_g is the group velocity and $\frac{1}{\tau}$ is the decay rate of energy inside the ring (which depends mainly on the losses and coupling coefficient inside the resonator). S_i and k_1 are the input field and the coupling coefficient, respectively.

Also, the energy of the back-reflection mode changes as in eq. (2):

$$\frac{\mathrm{db(t)}}{\mathrm{dt}} = \left(\mathrm{j}\omega_0 - \frac{1}{\tau}\right)\cdot \mathrm{b(t)} - \mathrm{ju}\cdot \mathrm{a(t)}. \quad (2)$$

Based on (1) and (2), *a(t)* and *b(t)* can be obtained as in (3), (4) and (5):

$$\mathrm{a(t)} = \frac{-\mathrm{j}k_1\cdot \mathrm{S_i} - \mathrm{ju}\cdot \mathrm{b(t)}}{\mathrm{A}}, \quad (3)$$

$$\mathrm{A} = \mathrm{j}(\omega - \omega_o) + \frac{1}{\tau}, \quad (4)$$

$$\mathrm{b(t)} = \frac{-\mathrm{ju}\cdot \mathrm{a(t)}}{\mathrm{A}}. \quad (5)$$

And from (3) and (5), equation (6) is obtained:

$$\mathrm{a(t)} = \frac{-\mathrm{j}\cdot k_1\cdot \mathrm{A}}{\mathrm{A^2} + \mathrm{u^2}}\cdot \mathrm{S_i}. \quad (6)$$

Considering that β is the propagation constant in a waveguide of length *l*; the response of each port is as follows [17]:

i. Through-port spectral response (equations (7) and (8)):

$$\mathrm{S_t} = \mathrm{e}^{\mathrm{j}\beta \mathrm{l}}\left(\mathrm{S_i} - \mathrm{j}\cdot k_1\cdot \mathrm{a(t)}\right), \quad (7)$$

$$\left|\frac{\mathrm{S_t}}{\mathrm{S_i}}\right|^2 = \left|1 - \frac{{k_1}^2\cdot \mathrm{A}}{\mathrm{A^2} + \mathrm{u^2}}\right|^2. \quad (8)$$

ii. Drop-port spectral response (equations (9) and (10)):

$$\mathrm{S_d} = -\mathrm{j}\cdot k_2\cdot \mathrm{a(t)}, \quad (9)$$

$$\left|\frac{\mathrm{S_d}}{\mathrm{S_i}}\right|^2 = \left|\frac{k_1k_2\cdot \mathrm{A}}{\mathrm{A^2} + \mathrm{u^2}}\right|^2. \quad (10)$$

iii. Add-port response (reflectivity) (equations (11 – (13)):

$$\mathrm{S_a} = -\mathrm{j}\cdot k_2\cdot \mathrm{b(t)}, \quad (11)$$

$$\mathrm{S_a} = \frac{-k_1k_2\cdot \mathrm{u}}{\mathrm{A}}\cdot \mathrm{a(t)}, \quad (12)$$

$$\left|\frac{\mathrm{S_a}}{\mathrm{S_i}}\right|^2 = \left|\frac{k_1k_2\cdot \mathrm{u}}{\mathrm{A^2} + \mathrm{u^2}}\right|^2. \quad (13)$$

The behavior at resonance is given in equations (14), (15) and (16):

$$\left|\frac{S_t}{S_i}\right|^2 = \frac{\left[u^2 + \frac{1}{\tau^2} - \frac{{k_1}^2}{\tau}\right]^2}{\left[u^2 + \frac{1}{\tau^2}\right]^2}, \quad (14)$$

$$\left|\frac{S_d}{S_i}\right|^2 = \frac{\frac{{k_1}^2 {k_2}^2}{\tau^2}}{\left[u^2 + \frac{1}{\tau^2}\right]^2}, \quad (15)$$

and

$$\left|\frac{S_a}{S_i}\right|^2 = \frac{{k_1}^2 {k_2}^2 \cdot u^2}{\left[u^2 + \frac{1}{\tau^2}\right]^2}. \quad (16)$$

To obtain the scattering parameters,

$$Th_o = \left|\frac{S_t}{S_i}\right|^2, Dr_o = \left|\frac{S_d}{S_i}\right|^2, \text{and } Re_o = \left|\frac{S_a}{S_i}\right|^2,$$

where, Th_o, Dr_o and Re_o are the through, drop and back reflection values at resonance respectively.

From (15) and (16):

$$\frac{Dr_o}{Re_o} = \frac{1}{\tau^2 \cdot u^2}. \quad (17)$$

Then,

$$u^2 = \frac{1}{\tau^2} \cdot \frac{Re_o}{Dr_o}. \quad (18)$$

To obtain τ, the ratio of Eqs. (10) and (13) is taken at f_1 which is the frequency where $Re = \frac{1}{2} \cdot Re_o$. With some rearrangements, equation (19) results:

$$\tau = \frac{1}{\Delta\omega} \cdot \sqrt{\frac{2Dr}{Dro} - 1}. \quad (19)$$

Dr is the value of the drop response at f_1 and $\Delta\omega$ is the frequency difference between f_1 and the resonant frequency.

Given the value of τ, the back-reflection coefficient is expressed as in Equ. (20):

$$R = \frac{(\Delta\omega)^2 \cdot l^2}{vg^2} \cdot \frac{Dro \cdot Re_o}{\sqrt{2Dr - Dro}}. \quad (20)$$

Also, the coupling coefficients can be represented as in equations (21) and (22):

$${k_1}^2 = \frac{l}{v_g} \cdot \frac{1}{\tau} \cdot \frac{(R_{eo} + D_{eo})}{D_{eo}} \cdot \left[1 - \sqrt{Th_o}\right], \quad (21)$$

$${k_2}^2 = \frac{l}{v_g} \cdot \frac{1}{\tau} \cdot \frac{(R_{eo} + D_{eo})}{\left[1 - \sqrt{Th_o}\right]}. \quad (22)$$

Finally, the losses can be measured based on [24] as in equation (23):

$${k_p}^2 = \left[\frac{2 \cdot l}{v_g} \cdot \frac{1}{\tau}\right] - {k_1}^2 - {k_2}^2. \quad (23)$$

And the losses coefficient is given in equation (24):

$$\alpha = \frac{1}{l} \cdot [-10 \cdot \log(1 - {k_p}^2). \quad (24)$$

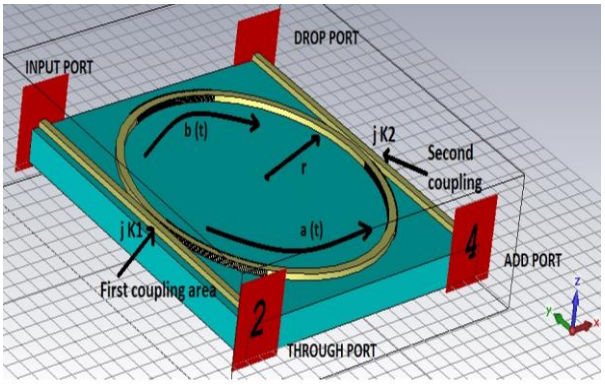

Fig. 1. Forward and back reflected modes in a rough-walled RR add/drop filter.

B. Space domain analysis

Although the scattering is distributed around the ring, it is helpful to think of it as an accumulated single scattering point [6] as shown in Fig. 2 (a). This point of scattering is characterized by $({K_r}^2)$ and $({t_r}^2)$, the back-reflection and transmission coefficient, respectively. The proposed equivalent structure is shown in Fig. 2 (b), where the reflection is assumed to be induced by a virtual ring.

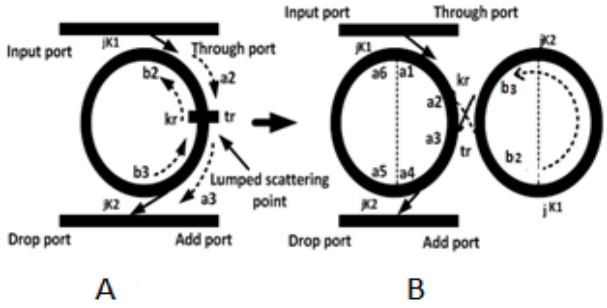

Fig. 2. The corrugated ring resonator (a), and (b) is the proposed virtual model.

The loop equations were written as in [17] to calculate the spectral responses of each port considering the existence of back reflection.

The drop port response is given in equation (25):

$$S_d = \frac{-k_1 k_2 \cdot \left[t_r - t_1 t_2 e^{-j\emptyset}\right] \cdot e^{-j\emptyset/2}}{1 - 2 \cdot t_1 t_2 \cdot t_r \cdot e^{-j\emptyset} + {t_1}^2 {t_2}^2 \cdot e^{-2j\emptyset}}, \quad (25)$$

where, $\emptyset = \alpha l + j\beta l$, is the propagation loss and phase change. k_1 and k_2 are the bus/ring power coupling coefficients, $t_r = \sqrt{1 - {k_r}^2}$ and l is the ring perimeter.

Also, the response of through port is given as in (26):

$$S_t = \frac{t - (t_1^2 - 1)t_r t_2 e^{-j\phi} + t_2^2 t_1 e^{-j\phi}}{1 - 2t_1 t_2 t_r e^{-j\phi} + (t_1 t_2)^4 e^{-2j\phi}}. \quad (26)$$

Finally, the induced back-reflected signal at the add port due to the counter directional propagated mode is as given in equation (27):

$$S_{back} = \frac{jk_r \cdot k_1 k_2 \cdot t_1 \cdot e^{-j3\phi/2}}{1 - 2 \cdot t_1 t_2 \cdot t_r \cdot e^{-j\phi} + {t_1}^2 {t_2}^2 \cdot e^{-2j\phi}}. \quad (27)$$

Equations (25) to (27) represent the frequency response of a corrugated ring OADM. These equations and equations (21)-(23) allow for complete modelling of corrugated ring resonators and provide an alternative solution to reproduce the experimental results without the need for curve fitting.

C. Validation

These models (in both the time and space domains) are examined first against the experimental outcomes published in [4].

1. The analytical model (time domain) represented by equations (20) to (23) is used to extract the coupling coefficients from the experimentally determined response presented in [4], as shown in Fig. 3 (b). The fitted parameters are: ${k_1}^2 = 4.8\%$, ${k_2}^2 = 1.76\%$, $t_r = 0.9991$ and the round-trip loss $e^{-\alpha l} = 0.9639$.

2. The space domain model was used to plot the spectral response and reproduce the experimental results using coupling coefficients (${K_1}^2, {K_2}^2, t_r$, and loss coefficient) calculated in step 1.

A comparison between Figs. 3 (a) and (b) shows the accuracy of the presented models and allows for the use of these equations for filter performance optimization in terms of crosstalk and signal integrity.

For further validation, a corrugated ring was modeled using CST MWS [21]. Figure 4 shows the CST model of a ring resonator based OADM.

In the electromagnetic model, the following parameters were used:

A substrate was silicon dioxide of 1 μm height with a 1.44 refractive index. Then the silicon waveguides were introduced above the substrate with 0.22 μm heights and 0.5 μm widths for single mode propagation [3]. A refractive index of 3.47 was used for the silicon waveguides [25]. The upper cladding was air. The corrugated ring was first modeled geometrically using Ruby code [26], and then moved into CST as a Wavefront.obj file. The ring radius was 8μm and the distances between the bus waveguides and the ring were 60 nm and 160 nm for the input and output bus waveguides, respectively. These values were taken to ensure the presence of resonance splitting. A hexahedral meshing in the transient CST solver was performed for simulation. The various spectral responses for the ports of a corrugated ring resonator are shown in Fig. 5. S_{21}, S_{31}, and S_{41} signify the output, drop and back reflection responses, respectively.

Equations (21) to (23) were used to calculate different parameters of the resonator from the simulation results. The modelled corrugated ring parameters (coupling, reflection, and loss coefficients) are calculated as: ${k_1}^2 = 10.774\%$, ${k_2}^2 = 1.422\%$, $t_r = 0.998$ and $e^{-\alpha l} = 0.986$.

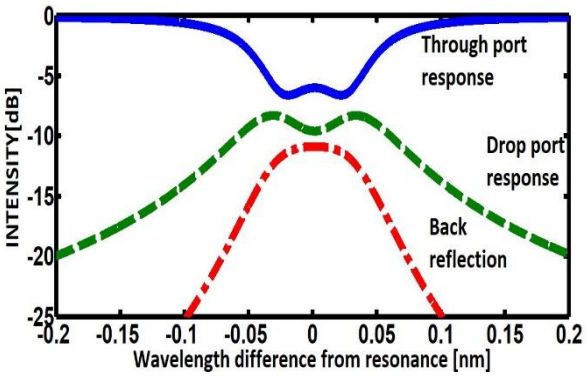

(a)

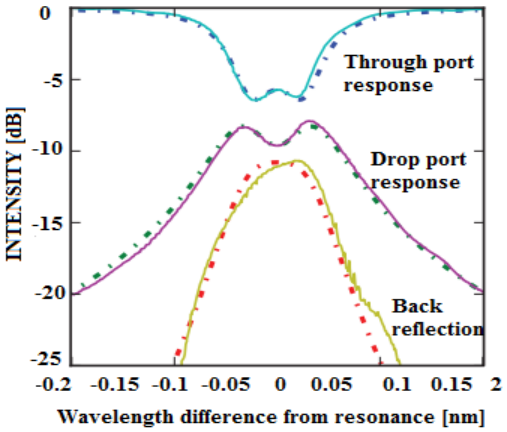

(b)

Fig. 3. (a) Spectral response of OADM based on time and space domain models. (b) Experimental results presented in [4].

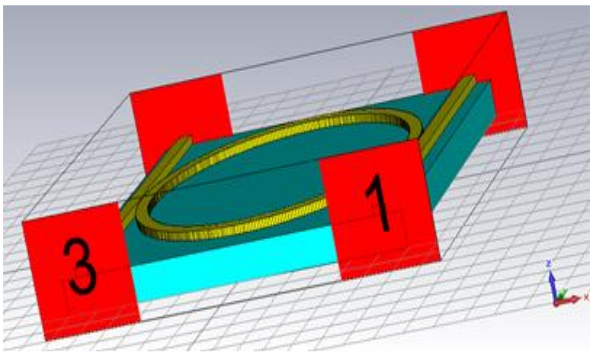

Fig. 4. CST model of a random sidewall roughness in a

corrugated single RR add /drop filter.

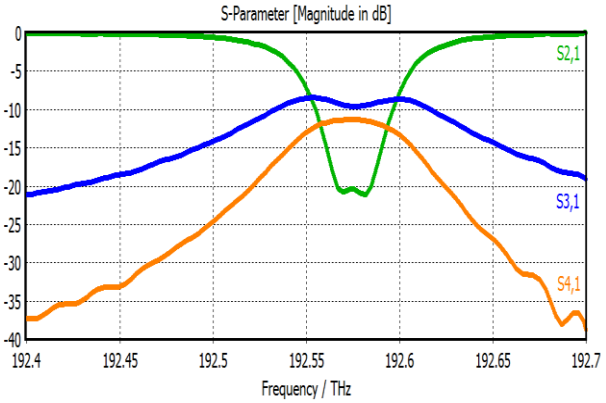

Fig. 5. CST spectral response of a corrugated ring.

These values were introduced into equations (25) - (27) to reproduce the spectral responses of different ports. Figure 6 shows a comparison between the analytically calculated port responses and that fitted using CST simulation. A good agreement between these results is clear. This provides additional validation for the derived equations and enables the application of them to study the effect of back-reflection on the crosstalk suppression bandwidth.

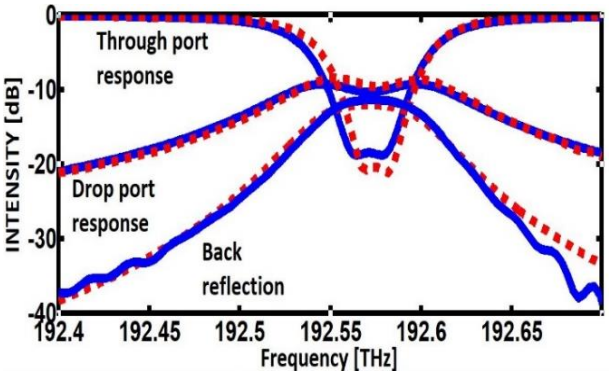

Fig. 6. Numerical (solid) and theoretical (dotted) modelled spectral response for a corrugated ring resonator.

Another advantage of the derived equations is in examining different values of the reflection coefficient (t_r) to show the effect of back-reflection on crosstalk suppression. Increasing the back-reflection coefficient, reducing t_r, leads to strong response splitting due to the mutual coupling between counter directional propagating modes, as shown in Fig. 7. Two minimums and a single maximum would exist in the output port response (S_{21}) of a single ring because of the back-reflection. Similarly, a double maximum and one minimum appears in the drop port response (S_{31}).

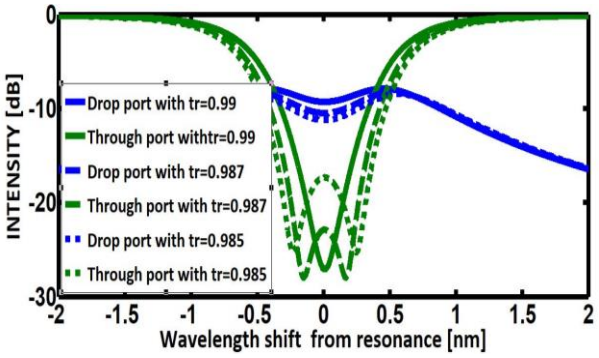

Fig. 7. The effect of reflection coefficient on the output and drop port response.

The difference between S31 (drop port response) and S21 (through port response) at each wavelength, represents the crosstalk suppression. It is required to be higher than |20| dB [27], for as wide a wavelength range as possible to increase the crosstalk suppression bandwidth to ensure high data rate channel dropping with improved signal integrity and mitigated crosstalk. This can be achieved by optimizing the reflectivity of the side-wall within the rough region, as discussed in the following sections.

III. CONTROLLABLE REFLECTIVITY

In this section, total reflectivity resulting from adding a number of reflectors is studied using the Bragg grating reflectivity model [15]. Single and double gratings are shown in Fig. 8.

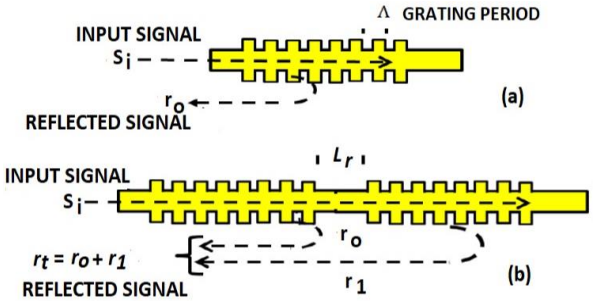

Fig. 8. (a) Single grating and (b) double gratings model.

The power back-reflection coefficient R is modelled as [28] and given in equation (28):

$$R = |r_0|^2 = \frac{k^2 \cdot \sinh^2(S \cdot L)}{\delta^2 \cdot \sinh^2(S \cdot L) + S^2 \cdot \cosh^2(S \cdot L)}, \quad (28)$$

where, r_0 is the reflection coefficient, $k = \frac{\pi \cdot \Delta n_{eff}}{\lambda}$ is the coupler coupling coefficient, and $\delta = \frac{2\pi n_{eff}}{\lambda} - \frac{\pi}{\Lambda}$, is the detuned propagation constant. n_{eff} is the effective refractive index, Λ is the period of the grating, L is the reflector length, and $S = \sqrt{k^2 - \delta^2}$. Equation (28) shows

a high dependency of the reflectivity on the change of n_{eff}, and grating parameters (L, and ʌ). Increasing the reflectivity by modifying various parameters is the main aim of this section. The refractive indices were 3.47 for Si and 1.44 for SiO_2 at the wavelengths around 1550 nm [3]. n_{eff} was 2.55, with a constant change over the grating as $\Delta n_{eff} = 0.5$. The effects of different parameters are examined as follows:

1. Reflector length (*L*): A 100 nm grating period and 50% duty cycle are considered first; these values were chosen to ensure high reflectivity around 1550 nm. Figure 9 shows that increasing L only influences a change of the reflectivity over the range of wavelengths around 1550 nm. Here, the range of wavelengths obtained was 1540-1560 nm and the best reflector length was 6500 nm (relatively high reflectivity) as shown in Fig. 9.

2. Grating period (ʌ): For $L = 6500$ nm and 50% duty cycle. Figure 10 shows an increase in the reflectivity with increasing grating period. Depending on the diffraction theory [12], the Bragg wavelength is ($\lambda_{Bragg} = 2 \cdot n \cdot \Lambda$). Therefore, increasing ʌ will increase the Bragg wavelength and shift it nearer to the required range.

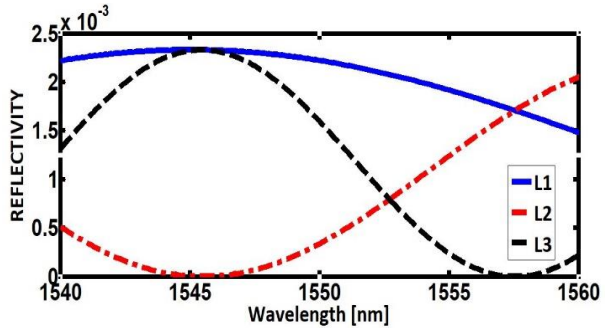

Fig. 9. The effect of ***L***. $L1$=6500 nm, L_2=13000 nm and L_3=19500 nm.

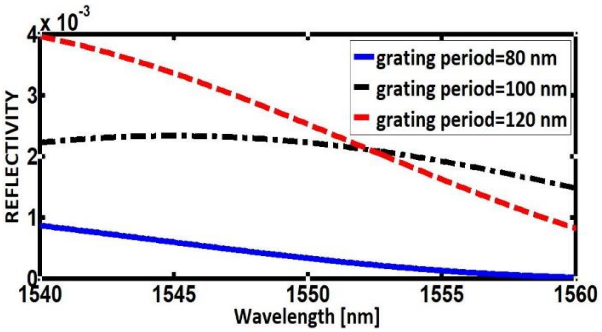

Fig. 10. The effect grating period.

3. Number of reflectors: Fig. 8 (b) shows the case of two groups of gratings, the total reflectivity of this model results from the contribution of each reflector. However, when adding r_0 and r_1, a locked loop needs to be considered between the reflectors. Based on Mason's rule [29], the total reflectivity of two reflectors is as given in equation (29):

$$r_0 + r_1 = \frac{r_0 + r_1 \cdot e^{-j2\beta L_r}}{1 + r_0 r_1 e^{-j\beta L_r}}. \quad (29)$$

For three groups of gratings, the total reflectivity will be greater due to the number of reflectors. The total reflectivity can be calculated as in equation (30):

$$r_0 + r_1 + r_2 = \frac{r_0 + r_1 e^{-j2\beta L_{r1}} + r_2 e^{-l2\beta(L_{r1}+L_{r2})} + r_0 r_1 r_2 e^{-j2\beta L_{r2}}}{1 + r_0 r_1 e^{-j2\beta L_{r1}} + r_1 r_2 e^{-j2\beta L_{r2}} + r_0 r_2 e^{-l2\beta(L_{r1}+L_{r2})}}, \quad (30)$$

where L_{r1} and L_{r2} are the separations between gratings. The reflectivity of one, two and three gratings is shown in Fig. 11.

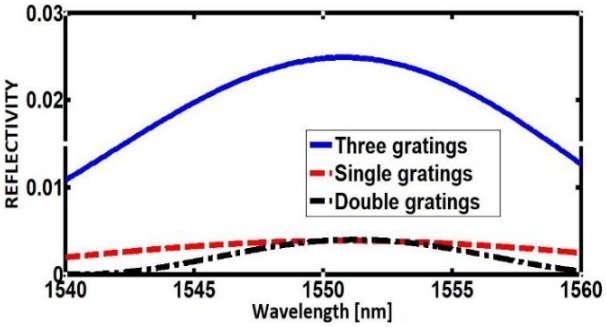

Fig. 11. Number of reflectors effect.

ASPIC design software [22] was used to validate equations (29) and (30), as shown in Fig. 12. ASPIC is a model-based simulation software and approaches simulation differently to the physically based CST MWS simulation software. The effect of using single, double and three gratings is simulated first. It is shown in Fig. 12 (b) that, increasing the number of gratings will result in an increase of back reflection as in [12]. Differences between analytical and ASPIC simulator results may be attributed to the change of the effective index with wavelength (material dispersion) [30].

4. Effect of *Lr*: to obtain high reflectivity, the distance between reflectors should ensure a π radian phase shift. The overall reflectivity is strongly affected by Lr as shown in Fig. 13. Therefore, the perimeter of the grating assisted ring needs to be optimized to maximize the reflection by ensuring a proper Lr.

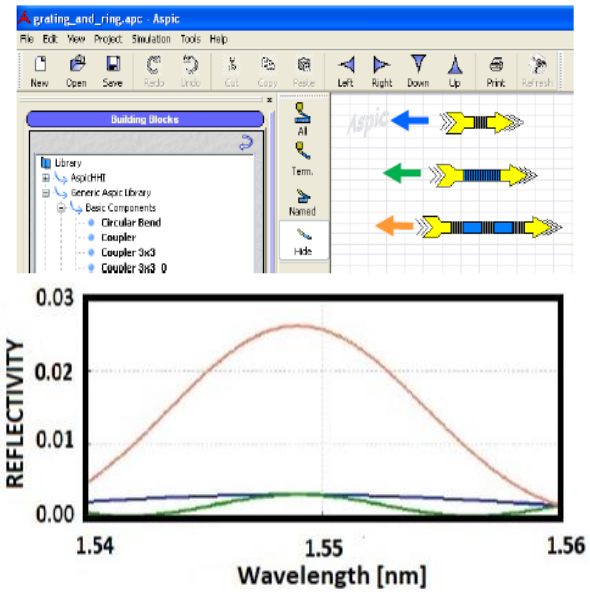

Fig. 12. Aspic model for three gratings (upper), and the reflectivity as a function of wavelength (lower) for single grating (blue), double grating (green) and three gratings (red).

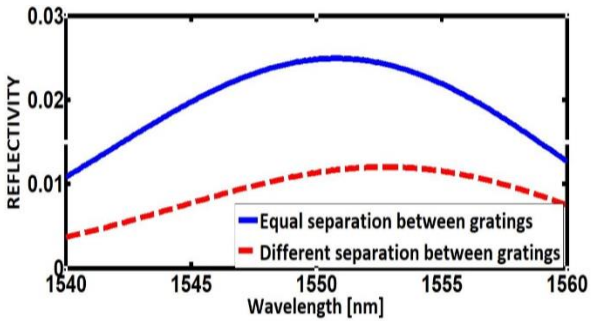

Fig. 13. The separation effect between three reflectors.

IV. GRATING ASSISTED SINGLE RING

This section aims to build on the above calculations to suggest a novel design of OADM that provides high crosstalk mitigation and ensure high integration density. The design steps are listed below:

Step 1: The goal-maximization algorithm is exploited to optimize the coupling and reflection coefficients that maximize the bandwidth of crosstalk suppression. Different parameters of an OADM with a corrugated ring are optimized based on Equations (25) and (26) to maximize the bandwidth of crosstalk suppression. Each time, a set of coupling coefficients (k_1, k_2 and tr) is used to calculate S_{31}-S_{21} and compare it with a |20| dB suppression threshold over the range of frequencies around one resonance.

Step 2: Not only k_1, k_2 and t_r need to be optimized, the ring radius needs to be chosen to match the resonance wavelength with the calculated value of tr.

Step 3: Three reflectors were used to ensure high reflectivity. The distance between the three reflectors was calculated as $(L_r = ((l - 3 \times L))/3)$, where l is the mean length of the ring. To maximize the reflectivity, the distance between reflectors was to be optimized.

Step 4: A model that combined all the parameters (coupling coefficients, ring radius, number of gratings, grating length, and grating period) was used. The optimization approach was performed for 100 and 120 mm grating period since these values provided increased reflectivity, as depicted in Fig. 10.

The optimized ring parameters for maximum crosstalk bandwidth in an asymmetric ring resonator were as follows: The power coupling coefficients ${K_1}^2 = 0.2258$, ${K_2}^2 = 0.0329$, and the back-reflection coefficient $t_r = 0.99$. The optimized value of back-reflection coefficient was used in equation (28) to calculate the length of reflectors inside the ring. A ring of 9.64 μm radius loaded with three reflectors each of 6.5μm length, separated by 13.7 μm is proposed. The period of ridges in each reflector is 0.1μm. A 28 GHz crosstalk suppression BW was obtained using these optimized parameters, as shown in Fig. 14. By comparison, an OADM made of a smooth surface ring with high coupling coefficient > 0.65 [18] is needed to obtain a similar crosstalk BW. Such a high coupling coefficient would affect the selectivity of the multiplexer (Q-factor) and allow for the adjacent channels to increase the inter-band crosstalk. Also, a double ring resonator can have a similar BW [18]. However, the integration density will be reduced due to the increased filter size.

To this extent it is shown analytically that a single ring with three reflectors provides high data-rate channel dropping compared to the smooth surface ring OADMs. To ensure the accuracy of the results, a numerical validation using ASPIC simulator for the proposed model was performed.

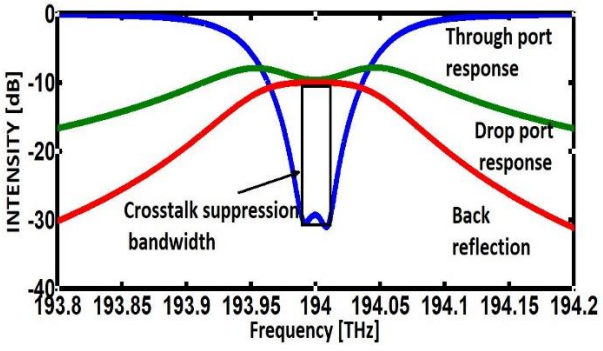

(a)

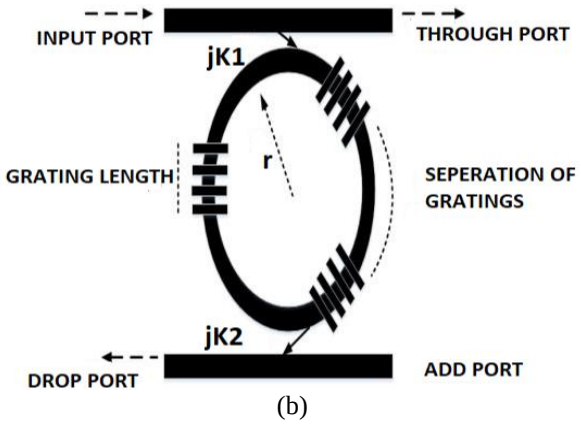

(b)

Fig. 14. (a) The single ring resonator spectral response, and (b) schematic of a grating-assisted OADM.

The ASPIC simulator results for a single ring resonator with three reflectors are shown in Fig. 15, which shows a good agreement with that of [17] (ASPIC simulation was performed for a 5 μm ring resonator model) where the resonance splitting is clear and |20| dB crosstalk suppression is maintained for a wide crosstalk suppression bandwidth.

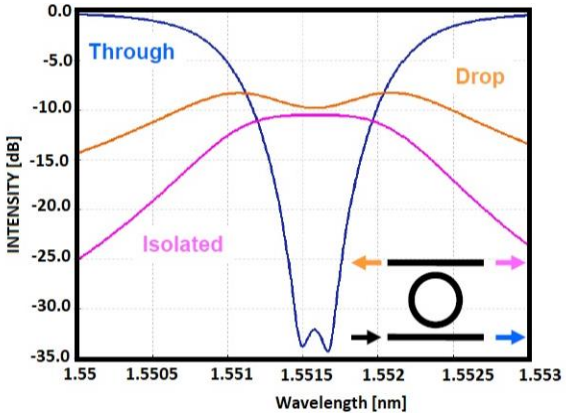

Fig. 15. The three-port response for a grating assisted ring resonator (Aspic simulated results).

V. CONCLUSION

Mitigating crosstalk effects and enhancing signal integrity in a small size ring resonator based OADM, by increasing the crosstalk suppression bandwidth, was the main aim of this paper. The objective of this work is to exploit the resonance splitting induced by silicon waveguide surface corrugation. To do that, a simple and direct approach to estimate all port responses without the need for curve fitting was presented. An equivalent model for the corrugated ring was proposed and examined against experimental published results. 3D simulation software was used for further validation. Analytical and numerical calculations were performed to ensure the accuracy of the proposed model. Finally, this model was used to obtain the optimized parameters of a ring resonator that maximize crosstalk suppression BW. A novel design, with more controllability during manufacture compared to a purely randomized corrugation, was proposed, and a 28 GHz crosstalk suppression BW was achieved. This bandwidth supports the dropping of 10 Gbps signals with mitigated crosstalk level and improved signal integrity.

REFERENCES

[1] A. Bianco, et al., "Crosstalk minimization in microring-based wavelength routing matrices," in *Global Telecommunications Conference (GLOBECOM), IEEE*, pp. 1-5, 2011.

[2] S. Koziel and S. Ogurtsov, "Simulation-driven optimization approach for fast design of integrated photonic components," in *30th Annual Review of Progress in Applied Computational Electromagnetic*, Jacksonville, FL, pp. 679-684, 2014.

[3] W. Bogaerts, et al., "Silicon microring resonators," *Laser & Photonics Reviews*, vol. 6, no. 1, pp. 47-73, 2012.

[4] G. Ballesteros, et al., "Characterizing and modeling backscattering in silicon microring resonators," *Optics Express*, vol. 19, no. 25, pp. 24980-24985, 2011.

[5] C. Sui, et al., "Analysis of microdisk/microring's surface roughness effect by orthogonal decomposition," *Optics and Photonics Journal*, vol. 3, pp. 288, 2013.

[6] B. E. Little, J. Laine, and S. T. Chu, "Surface-roughness-induced contradirectional coupling in ring and disk resonators," *Opt. Lett.*, vol. 22, no. 1, pp. 4-6, 1997.

[7] Z. Zhang, et al., "Resonance-splitting and enhanced notch depth in SOI ring resonators with mutual mode coupling," *Optics Express*, vol. 16, no. 7, pp. 4621-4630, 2008.

[8] G. T. Paloczi, J. Scheuer, and A. Yariv, "Compact microring-based wavelength-selective inline optical reflector," *IEEE Photonics Technology Letters*, vol. 17, no. 2, pp. 390-392, 2005.

[9] C. Alonso-Ramos, et al., "Dual-mode coupled-resonator integrated optical filters," *IEEE Photonics Technology Letters*, vol. 26, pp. 929-932, 2014.

[10] R. D. Mansoor, et al., "Estimation of the bandwidth of acceptable crosstalk of parallel coupled ring resonator add/drop filters," *IEEE Trans. Electromagn. Compat.*, vol. 57, no. 5, pp. 1005-1012, 2015.

[11] F. Morichetti, A. Canciamilla, and A. Melloni, "Statistics of backscattering in optical waveguides," *Opt. Lett.*, vol. 35, no. 11, pp. 1777-1779, 2010.

[12] T. Wang, et al., "Modeling of quasi-grating sidewall corrugation in SOI microring add-drop

filters," *Opt. Commun*., vol. 282, no. 17, pp. 3464-3467, 2009.
[13] Y. M. Kang, A. Arbabi, and L. L. Goddard, "Engineering the spectral reflectance of microring resonators with integrated reflective elements," *Optics Express*, vol. 18, no. 16, pp. 16813-16825, 2010.
[14] W. Shi, et al., "Grating-coupled silicon microring resonators," *Appl. Phys. Lett*., vol. 100, no. 12, pp. 121118-121118-4, 2012.
[15] K. O. Hill and G. Meltz, "Fiber Bragg grating technology fundamentals and overview," *J. Lightwave Technol*., vol. 15, no. 8, pp. 1263-1276, 1997.
[16] A. E. Atia and A. E. Williams, "Narrow-bandpass waveguide filters," *Microwave Theory and Techniques, IEEE Transactions On*, vol. 20, no. 4, pp. 258-265, 1972.
[17] R. Mansoor, et al., "Crosstalk bandwidth of grating-assisted ring resonator add/drop filter," *Opt. Quant. Electron*., vol. 47, pp. 1127-1137, 2015.
[18] R. D. Mansoor, et al., "Over coupled ring resonator based add/drop filters," *Quantum Electronics, IEEE Journal of*, vol. 50, no. 8, pp. 598-604, 2014.
[19] A. Yariv, "Coupled-mode theory for guided-wave optics," *Quantum Electronics, IEEE Journal of*, vol. 9, no. 9, pp. 919-933, 1973.
[20] O. Schwelb, "Microring resonator based photonic circuits: Analysis and design," in *Telecommunications in Modern Satellite, Cable and Broadcasting Services*, pp. 187-194, 2007.
[21] 3D Electromagnetic Simulation software, 2013. Available: www.cst.com.
[22] ASPIC design software, 2014. Available: www.aspicdesign.com.
[23] C. Manolatou, et al., "Coupling of modes analysis of resonant channel add-drop filters," *Quantum Electronics, IEEE Journal of*, vol. 35, no. 9, pp. 1322-1331, 1999.
[24] S. Xiao, et al., "Modeling and measurement of losses in silicon-on-insulator resonators and bends," *Optics Express*, vol. 15, no. 17, pp. 10553-10561, 2007.
[25] O. Schwelb, "Transmission, group delay, and dispersion in single-ring optical resonators and add/drop filters-a tutorial overview," *Lightwave Technology, Journal of*, vol. 22, no. 5, pp. 1380-1394, 2004.
[26] Ruby programming language. 2014. Available: https//:www.ruby-lang.org
[27] O. Schwelb, "Crosstalk and bandwidth of lossy microring add/drop multiplexers," *Opt. Commun*., vol. 265, no. 1, pp. 175-179, 2006.
[28] S. P. Ugale and V. Mishra, "Modeling and characterization of fiber Bragg grating for maximum reflectivity," *Optik-International Journal for Light and Electron Optics*, vol. 122, no. 22, pp. 1990-1993, 2011.
[29] S. J. Mason, *Feedback Theory: Further Properties of Signal Flow Graphs*. Research Laboratory of Electronics, Massachusetts Institute of Technology, 1956.
[30] H. Li, "Refractive index of silicon and germanium and its wavelength and temperature derivatives," *Journal of Physical and Chemical Reference Data*, vol. 9, no. 3, pp. 561-658, 1980.

Riyadh D. Mansoor received the B.Sc degree in Electrical and Electronic Engineering and the Master degree from the University of Basra, Iraq, in 1996 and 1998 respectively. He finished his Ph.D. in Optical Communication at De Montfort University, Leicester, UK, in 2015. He is currently working as a Senior Lecturer with the faculty of Engineering, Al-Muthanna University, Samawa, Iraq. His research interests include photonic circuits, optical communications, and Electromagnetic compatibility.

Alistair P. Duffy received the B.Eng. (Hons.) degree in Electrical and Electronic Engineering and the M.Eng. degree from University College, Cardiff, U.K., in 1988 and 1989, respectively. He received his Ph.D. degree from Nottingham University, Nottingham, U.K., in 1993 for his work on experimental validation of numerical modeling.

He is currently Professor of Electromagnetics and Director of the Institute of Engineering Sciences at De Montfort University, Leicester, U.K. He is also a Guest Professor at Harbin Institute of Technology, Harbin, China. He is the author of approximately 300 articles published in journals and presented at international symposia. His research interests include CEM validation, communications cabling, and technology management.

Duffy is a Fellow of the IEEE, the Institution of Engineering and Technology (IET) and the Royal Society for the Encouragement of Arts, Manufactures and Commerce (RSA). He is currently President Elect for the IEEE EMC Society. He is also Chair of the IEEE EMC Society Standards Development and Education Committee, along with a number of Standards working group officer roles. He is an Associate Editor of the IEEE Transactions on EMC Technology management.